Antimicrobial Agents and Chemotherapy

Plasmodium Dipeptidyl Aminopeptidases as Malaria Transmission-Blocking Drug Targets

Takeshi Q Tanaka, Edgar Deu, Alvaro Molina-Cruz, Michael J. Ashburne, Omar Ali, Amreena Suri, Sandhya Kortagere, Matthew Bogyo and Kim C. Williamson

Antimicrob. Agents Chemother. **2013, 57(10):4645. DOI: 10.1128/AAC.02495-12.**
Published Ahead of Print 8 July 2013.

AAC Journals.ASM.org

Plasmodium Dipeptidyl Aminopeptidases as Malaria Transmission-Blocking Drug Targets

Takeshi Q Tanaka,[a] Edgar Deu,[b]* Alvaro Molina-Cruz,[a] Michael J. Ashburne,[c] Omar Ali,[c] Amreena Suri,[c] Sandhya Kortagere,[d] Matthew Bogyo,[b] Kim C. Williamson[a,c]

Laboratory of Malaria and Vector Research, National Institute of Allergy and Infectious Diseases, National Institutes of Health, Rockville, Maryland, USA[a]; Department of Pathology, Stanford School of Medicine, Stanford, California, USA[b]; Department of Biology, Loyola University Chicago, Chicago, Ilinois, USA[c]; Department of Microbiology and Immunology, Drexel University College of Medicine, Philadelphia, Pennsylvania, USA[d]

The *Plasmodium falciparum* and *P. berghei* genomes each contain three dipeptidyl aminopeptidase (*dpap*) homologs. *dpap1* and -3 are critical for asexual growth, but the role of *dpap2*, the gametocyte-specific homolog, has not been tested. If DPAPs are essential for transmission as well as asexual growth, then a DPAP inhibitor could be used for treatment and to block transmission. To directly analyze the role of DPAP2, a *dpap2*-minus *P. berghei* (*Pbdpap2Δ*) line was generated. The *Pbdpap2Δ* parasites grew normally, differentiated into gametocytes, and generated sporozoites that were infectious to mice when fed to a mosquito. However, *Pbdpap1* transcription was >2-fold upregulated in the *Pbdpap2Δ* clonal lines, possibly compensating for the loss of *Pbdpap2*. The role of DPAP1 and -3 in the *dpap2Δ* parasites was then evaluated using a DPAP inhibitor, ML4118S. When ML4118S was added to the *Pbdpap2Δ* parasites just before a mosquito membrane feed, mosquito infectivity was not affected. To assess longer exposures to ML4118S and further evaluate the role of DPAPs during gametocyte development in a parasite that causes human malaria, the *dpap2* deletion was repeated in *P. falciparum*. Viable *P. falciparum dpap2* (*Pfdpap2*)-minus parasites were obtained that produced morphologically normal gametocytes. Both wild-type and *Pfdpap2*-negative parasites were sensitive to ML4118S, indicating that, unlike many antimalarials, ML4118S has activity against parasites at both the asexual and sexual stages and that DPAP1 and -3 may be targets for a dual-stage drug that can treat patients and block malaria transmission.

Malaria remains a major global health problem, and the emergence of multidrug-resistant strains serves as a reminder that additional approaches are essential for malaria control and eradication (1). The development of drugs that block transmission by killing sexual-stage parasites, called gametocytes, is a key part of this strategy (2–4). Once ingested by a mosquito, gametocytes emerge from the host red blood cells (RBCs) as male and female gametes that undergo sexual reproduction, leading to the development of sporozoites that can infect humans during a mosquito blood meal (5). Most commonly used antimalarials do not have strong gametocytocidal activity at therapeutic concentrations (6), allowing the parasites to be transmitted for more than a week after the clearance of asexual parasites. The identification of new targets and gametocytocidal compounds is needed to advance the development of transmission-blocking drugs (6–8).

Both gametocytes and asexual parasites develop inside human erythrocytes and digest host hemoglobin as their initial primary nutrient source. Consequently, the pathways involved in hemoglobin degradation and the detoxification of the resulting heme by polymerization make reasonable drug targets (9). Hemoglobin is initially degraded to oligopeptides in the food vacuole by endoproteases, including falcipain, plasmepsin I, II, and IV, falcilysin, and histoaspartic protease, and then further digested by exopeptidases (10, 11). Dipeptidyl aminopeptidase 1 (DPAP1) is one exopeptidase which localizes to the food vacuole and cleaves dipeptides from the amino termini of proteins or oligopeptides (12, 13). There are three DPAP homologs in *Plasmodium* species that infect humans and rodents. DPAP1 and -3 are suggested to be involved in hemoglobin degradation and egress from RBCs, respectively (14, 15), and DPAP1 is considered to be essential, as shown by inhibitor studies and its inability to be genetically deleted (13). *dpap2* is transcribed only in gametocytes (16), and its role remains unknown since the gametocyte and mosquito stages were not included in the initial inhibitor analysis (15). Since hemoglobin digestion is essentially complete by stage III of gametocytogenesis (17, 18). DPAP2 might have a role in alternative metabolic pathways in late-stage gametocytes and during sporogonic development in the mosquito. These alternative pathways have not yet been defined, and the identification of genes that are essential to these transmission stages could contribute to their elucidation. If DPAPs have a critical role in mosquito and asexual stages, inhibitors could be used to treat patients and also to block transmission.

In this work, the role of DPAP2 was tested directly by targeted gene disruption in both *Plasmodium berghei* and *P. falciparum*. The use of the rodent malaria, *P. berghei*, allowed analysis of the entire life cycle, including mouse-to-mouse transmission via a mosquito, while the human malaria, *P. falciparum*, allowed the evaluation of gametocyte development in *in vitro* culture. Additionally, unlike most other *Plasmodium* species which require 1 to 2 days to produce spherical gametocytes, *P. falciparum* gametocytes require 10 days and progress through 5 distinct morpholog-

Received 12 December 2012 Returned for modification 10 April 2013
Accepted 2 July 2013
Published ahead of print 8 July 2013
Address correspondence to Kim C. Williamson, kwilli4@luc.edu.
* Present address: Edgar Deu, Division of Parasitology, MRC National Institute for Medical Research, London, United Kingdom.
Supplemental material for this article may be found at http://dx.doi.org/10.1128/AAC.02495-12.

doi:10.1128/AAC.02495-12

ical stages, providing a prolonged time course to evaluate function. Inhibitors and control compounds were used to study the role of DPAP1 and -3 in the transmission stages, since neither gene has been successfully deleted. The findings suggest that DPAP proteases could be targets for a "two-way" drug that can be used for both patient treatment and transmission blocking.

MATERIALS AND METHODS

Experimental animals. The Swiss Webster mice (4 to 6 weeks old) used in the experiments were supplied by Harlan or Charles River Laboratories International, Inc. All animal experiments were approved by the Institutional Animal Care and Use Committees at Loyola University Chicago or the National Institute of Allergy and Infectious Diseases.

***Pbdpap2* deletion in *P. berghei*.** Two sections of *P. berghei dpap2* (*Pbdpap2*) (PBANKA_146070; http://plasmodb.org/plasmo/) were amplified by PCR from *P. berghei* ANKA 234 genomic DNA (gDNA) using the primers listed in Table S1 in the supplemental material. The 5′ region extended from 420 bp upstream of the ATG to 524 bp downstream, while the 3′ section included bp 2510 to 2836. Both sections included introns. The 5′ and 3′ PCR products were digested with ApaI and HindIII and with XbaI and SacII, respectively, and inserted sequentially into the corresponding sites in pL0001 vector (http://www.mr4.org). The sequence of the plasmid containing both inserts was confirmed, and then the plasmid was linearized using SacII. *P. berghei* parasites, ANKA strain, were transformed with the linearized construct following the Nucleofector (Lonza) protocol described by Janse et al. (19) and used to inoculate mice by intravenous injection. The mice were provided drinking water containing pyrimethamine (10 μg ml^{-1}) to select for transformed parasites. The pyrimethamine-resistant parasites obtained were analyzed for gene deletion and then cloned by limiting dilution passage into naive mice. The clonal *Pbdpap2*Δ lines were then used to infect naive mice to analyze asexual growth, gametocyte production, and transmission to mosquitoes. Mosquitoes fed on the infected mice were maintained at 21°C for 3 weeks and then allowed to feed on naive mice to test the ability of the *Pbdpap2*Δ clones to produce infectious sporozoites and complete the life cycle.

***Plasmodium falciparum* parasite culture and gametocyte production.** *Plasmodium falciparum* parasites were maintained in *in vitro* culture using the protocol developed by Trager and Jensen (20). Gametocytes were produced by maintaining the culture for 16 days by feeding daily with RPMI 1640 supplemented with 10% serum but not adding additional RBCs. This method was first described by Ifediba and Vanderberg (21).

***Pfdpap2* deletion.** A section of *P. falciparum dpap2* (*Pfdpap2*) (PF3D7_1247800; http://plasmodb.org/plasmo/) corresponding to nucleotides 1537 to 2203 which includes the 3′ end of exon 6 and of exon 7 and the 5′ end of exon 8 was amplified by PCR from *P. falciparum* strain 3D7 gDNA using the primers indicated in Table S1 in the supplemental material and inserted into the ApaI and EcoRV sites that had been added to pDT.Tg23 as described previously (22). After the sequence was confirmed, purified plasmid (Qiagen Maxi Prep) was used to transform *P. falciparum* (3D7 strain) using established procedures (22). Following electroporation, the parasites were returned to culture in RPMI 1640 supplemented with 10% serum under the standard conditions (37°C in 90% nitrogen, 5% CO_2, and 5% O_2) (20). Starting on the third day, the parasites were treated with 100 ng ml^{-1} pyrimethamine for 48 h and then maintained on 15 ng ml^{-1} to select for resistant parasites. The resistant parasites were cloned by limiting dilution and assayed for gene disruption as described below.

DNA and RNA analysis. gDNA was extracted and purified from saponin-treated *P. falciparum* cultures using a Wizard genomic DNA purification kit (Promega). gDNA from *P. berghei* and *P. falciparum* was treated with ClaI and KpnI, respectively. The digested gDNA was size fractionated on an agarose gel and analyzed by Southern hybridization using probes amplified by PCR with the primers indicated in Table S1 in the supplemental material.

RNA was isolated from *P. falciparum* gametocytes using TRIzol (Life Technologies, Carlsbad, CA) according to the manufacturer's instructions (23). The purified total RNA was size fractionated using formaldehyde-agarose gel electrophoresis and analyzed by Northern hybridization using probes amplified by PCR with the primers indicated in Table S1 in the supplemental material.

RT-qPCR. *P. berghei* schizonts were isolated from the rings and trophozoites by Nycodenz density gradient centrifugation (19), and gametocytes were isolated from parasitemic mice following 48-h sulfadiazine treatment to clear asexual parasites. Total RNA was extracted using TRIzol and then purified using an RNeasy Micro kit (Qiagen) according to the manufacturer's instructions. In addition to DNase treatment during RNA isolation on the Micro columns, purified RNA (50 ng) was treated with gDNA wipeout buffer before conversion to cDNA using QuantiTect reverse transcriptase (RT) (Qiagen). RT-minus controls were included to confirm the absence of gDNA. The cDNA from the RT-plus reactions was used as a template for quantitative PCR (RT-qPCR) (StepOnePlus; Applied Biosystems) with the indicated primers (see Table S1 in the supplemental material) and SYBR green PCR Master Mix (Applied Biosystems) using the following conditions: 5 min activation at 95°C and 40 cycles of 10 s at 95°C and 30 s at 60°C. All samples were run in triplicate and tested for both the gene of interest and the control constitutive gene, A-type 18S rRNA (berg07_18S; http://plasmodb.org/plasmo/) (24), on the same plate. The results were analyzed using StepOnePlus V 2.2 software (Applied Biosystems), and the ΔC_T values were determined by subtracting the mean threshold cycle (C_T) values of the target gene and constitutive control gene. The relative abundance in the *dpap2*Δ samples in comparison to that in the wild-type samples was calculated ($2^{-\Delta\Delta CT}$) and the log2 plotted.

***In vitro* DPAP enzymatic assay.** *P. berghei* schizonts and gametocytes were prepared as described above for the RT-qPCR assay. DPAP activity was evaluated with a cell-permeative, fluorescently tagged probe (FY01) that covalently modifies the catalytic cysteine of the active form of DPAPs (14). Parasite pellets were lysed for 1.5 h in 1% NP-40–PBS at 0°C and diluted 1/10 in acetate buffer (pH 5.5), and enzymatic activity was measured by incubating the lysates with 1 μM FY01 for 1 h at 25°C. The reaction was stopped by the addition of SDS-PAGE loading buffer and incubation at 95°C for 5 min. The samples were size fractioned, and the FY01-labeled proteases were visualized using a flatbed fluorescence scanner. DPAP inhibition was measured using a competition assay in which lysates were incubated with inhibitor for 30 min prior to FY01 labeling (14, 15). Serial dilutions were used to determine the 50% inhibitory concentration (IC_{50}) of selected compounds (14, 15).

***P. berghei* growth and exflagellation assay.** Three mice were inoculated with 1×10^6 *P. berghei* wild-type or *Pfdpap2*Δ parasites by intraperitoneal injection on day 1. Giemsa-stained smears were prepared, and exflagellation was tested every day from day 2 to day 15. Briefly, for the exflagellation assays, blood samples (2 μl) were mixed with 7 μl of RPMI supplemented with 20% fetal bovine serum (FBS) and 1 μl of 40 IU ml^{-1} heparin solution (total 10 μl). The mixture was incubated at 19°C for 15 min to induce exflagellation and then monitored by microscopy to quantify exflagellation centers and total RBCs per field at ×400 magnification.

***In silico* protein structure modeling.** The protein sequences of *P. falciparum* DPAPs (DPAP1 to -3) were obtained from http://plasmodb.org/plasmo/ with accession numbers PF3D7_1116700, PF3D7_1247800, and PF3D7_0404700. Multiple alignment of the three sequences revealed significant differences in their lengths, with DPAP1 and DPAP3 having large insertions that could lead to deviations in their three-dimensional structures in comparison to DPAP2. Based on this observation, DPAP1 and DPAP2 were chosen for homology modeling using the crystal structure of human cathepsin C (hCAT-c) in complex with Gly-Phe-diazomethane inhibitor (Protein Data Bank [PDB] code 2DJF; http://www.pdb.org/pdb/files/2DJF.pdb) (25) as the template for homology modeling program MODELLER version 9.0 (26). The resulting models of DPAP1 and -2 were subjected to further refinement using NAMD2 (27). Since the DPAP1 structure had a 55-residue-long insertion that had no homology

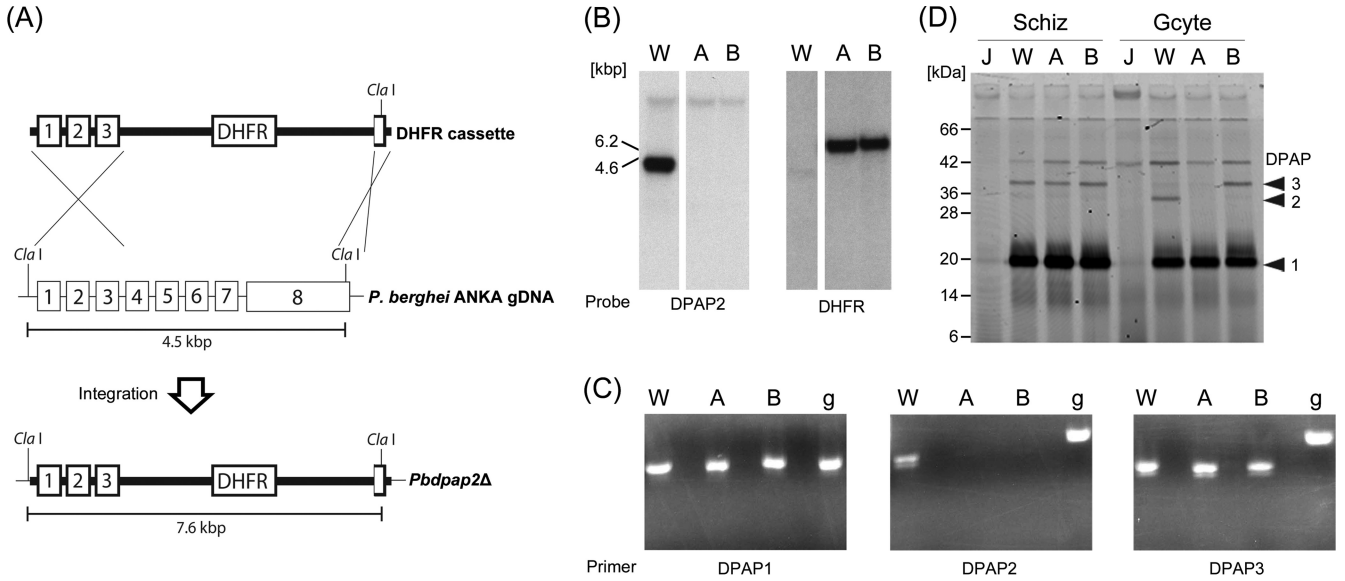

FIG 1 *P. berghei dpap2* deletion. (A) Schematic of the *Pbdpap2*Δ locus in *P. berghei*. (B) Southern blotting of ClaI-digested gDNA demonstrating the replacement of *Pbdpap2* with the DHFR cassette integration. W, wild type; A, *Pbdpap2*Δ clone A; B, *Pbdpap2*Δ clone B. (C) RT-PCR of mixed-stage samples demonstrating *Pbdpap1*, *-2*, and -3 in wild-type gDNA (g) and the absence of *Pbdpap2* in the *Pbdpap2*Δ clones. (D) DPAP enzymatic assay based on the covalent labeling of the indicated schizont (Schiz) or gametocyte (Gcyte) extracts with fluorescent substrate FY01. Asexual parasites were not completely eliminated from the *Pbdpap2*Δ clone B gametocyte preparation. Lane J contains wild-type parasite treated with 1 μM JCP410, a general DPAP inhibitor, as a negative control.

to the hCAT-c structure, this region was not modeled and the ends were capped before being subjected to refinement. The structure refinement consisted of routines for energy minimization followed by molecular dynamics simulation with a production run of 1 ns. ML4118S was modeled using the builder module of Molecular Operating Environment (MOE) (Chemical Computing Group) and geometry optimized using MOPAC with the AM1 basis set as adopted in MOE. The molecule was then docked to the S2 site of DPAP1 and -2 structures using GOLD docking software (28).

Membrane feeding to mosquitoes and oocyst production. In advance of the mosquito feed experiments, all equipment and solutions were warmed at 37°C. Blood (600 μl) was collected from mice infected with *Pbdpap2*Δ clone A and added to 5 ml of RPMI 1640 media supplemented with 0.8 IU ml^{-1} heparin. The cells were isolated by centrifugation (800 × *g* for 5 min) at room temperature, and the 300-μl cell pellet was resuspended in 450 μl of fetal bovine serum. Aliquots (200 μl) of the resuspended cells were incubated with 0.2 μl of 10 mM ML4118S or dimethyl sulfoxide (DMSO) for 10 min at 37°C before being fed to *Anopheles stephensi* using a membrane feeder. At 11 to 12 days later, the midguts of the mosquitoes were dissected and the numbers of mercurochrome-stained oocysts counted under ×400 magnification.

***P. falciparum* gametocytocidal assay.** The gametocytocidal assay was performed as described previously (6). In brief, purified stage III to V gametocytes (100 μl) were incubated with 1 μl of 3 mM ML4118S or ML4118R–DMSO at 30 μM final concentrations for 72 h on a 96-well plate without changing media. A 10-μl volume of alamarBlue was then added to each well, and the plate was returned to standard culture conditions for 24 h. The fluorescence of reduced alamarBlue in the supernatant was measured at 590/35 nm following excitation at 530/25 nm.

Statistical analysis. All statistical analysis was done with GraphPad Prism 5 software (GraphPad Software, Inc.).

RESULTS

Deletion of *dpap2* in *P. berghei*. *P. berghei dpap2*Δ parasite lines were obtained from two independent transformations after pyrimethamine selection and screened for replacement of *Pbdpap2* with the dihydrofolate reductase (DHFR) cassette by Southern blotting of ClaI-digested genomic DNA (Fig. 1A and B). After limiting dilution and reinjection into naive mice, 4 clonal parasite lines, 2 from each transformation, were obtained. Transcript analysis of parasites isolated from the wild type and from 2 independent *Pbdpap2*Δ clones, A and B, confirmed the lack of *Pbdpap2* mRNA in the *Pbdpap2*Δ clones, as well as the presence of *Pbdpap1* and -3 mRNA (Fig. 1C). The corresponding PCR product obtained from wild-type genomic DNA is shown in the last lane in each set and is larger than the RT-PCR product for *Pbdpap2* and -3 due to the presence of introns.

PbDPAP protein expression was evaluated by labeling with FY01, a fluorescent activity-based probe that covalently modifies the catalytic cysteine of the active form of DPAPs (Fig. 1D). Prior work in *P. falciparum* parasites demonstrated a dominant DPAP1 band at 20 kDa throughout the asexual cycle and three bands for DPAP3 at 120, 95, and 42 kDa in mature schizonts and merozoites (14). FY01-labeled *P. berghei* schizont extracts demonstrated a similar dominant band at 20 kDa consistent with PbDPAP1 and bands at 38 and 42 kDa. Wild-type *P. berghei* gametocytes have the 20- and 42-kDa bands as well as an additional band at 33 kDa that is not present in the schizont extract or in either of the *Pbdpap2*Δ clonal lines, suggesting that it corresponds to PbDPAP2. This size is consistent with the predicted molecular mass of the PbDPAP2 catalytic domain (31.4 kDa) when the prodomain cleavage site is similar to that observed for PfDPAP1 (13). The 38-kDa band, which is similar to the predicted size of the fully processed PbDPAP3 (37.2 kDa) based on the processing of PfDPAP1 (13), is present only in the gametocytes harvested from mice that did not receive a full course of sulfadiazine treatment to eliminate all the asexual parasites, suggesting that this band represents DPAP3, which is expressed primarily in schizonts.

The *Pbdpap2*Δ strain showed normal growth and completed the entire life cycle. To evaluate the effect of *Pbdpap2* deletion on

TABLE 1 Normal growth and exflagellation of *Pbdpap2*Δ clones[a]

Parameter	Avg (minimum–maximum) values					
	Expt 1			Expt 2		
	WT	KO clone A	KO clone B	WT	KO clone A	KO clone B
% maximum parasitemia	56.9 (35.6–90.8)	32.2 (3.5–60.1)	53.4 (39.7–62.1)	23.5 (8.5–34.7)	37.7 (30.1–44.0)	36.1 (11.6–49.1)
First day parasitemia was >1%	5.3 (5–6)	7.3 (5–10)	6.0 (6–6)	6.0 (5–7)	5.0 (5–5)	6.7 (6–8)
Maximum exf/10,000 cells	30.8 (16.9–57.3)	19.7 (14.6–25.5)	22.5 (11.5–42.9)	17.2 (8.5–26.5)	38.3 (10.8–87.5)	24.4 (8.9–44.7)
Maximum exf/100 iRBC	2.3 (1.9–3.5)	3.0 (1.1–4.8)	2.0 (1.0–3.5)	3.2 (2.9–3.5)	2.3 (1.2–3.1)	4.9 (2.7–8.7)
First day exf was observed	5.0 (4–6)	7.0 (5–10)	5.7 (5–6)	6.3 (6–7)	5.3 (4–7)	6.3 (5–8)

[a] Averages and, in parentheses, minimum and maximum values from 2 independent experiments (experiments 1 and 2) that each included 3 mice are shown. WT, wild-type parasites; KO clone A, *Pbdpap2*Δ clone A; KO clone B, *Pbdpap2*Δ clone B; exf, exflagellation center.

asexual growth and sexual maturation, the course of intraerythrocytic development of the wild type and of two *Pbdpap2*Δ clones was evaluated in 3 mice each. The maximum parasitemia, the day the parasitemia first exceeded 1% parasitemia, and the survival rate were recorded, as were the day exflagellation was first observed and the maximum number of exflagellation centers per 10,000 RBC cells or 100 parasite-infected RBCs (iRBCs) (Table 1; see also Fig. S1 in the supplemental material). Two-way analysis of variance (ANOVA) of the effect of strain and experiment, followed by Bonferroni's multiple comparative analysis, found no difference between the three strains or two experiments, indicating that the development of the *Pbdpap2*Δ clones in mice was the same as that of the wild type.

Analysis was extended to the entire life cycle by allowing mosquitoes to feed on mice infected with wild-type or *Pbdpap2*Δ parasites. To allow sufficient time for the development of infectious sporozoites, the mosquitoes were fed on naive mice 3 weeks later. Both wild-type and *Pbdpap2*Δ parasites were successfully transmitted to naive mice, indicating that *Pbdpap2* is not required for gametocytes to be transferred to mosquitoes, fertilize, and generate infectious sporozoites.

Transcripts for DPAPs in *Pbdpap2*Δ clones. The sequence similarity of all 3 *Pbdpap* forms raises the issue of whether the levels of *Pbdpap1* or -3 increase to compensate for the lack of *Pbdpap2*. Reverse transcriptase quantitative PCR (RT-qPCR) was used to compare the levels of *Pbdpap1* and -3 in the wild type and the *Pbdpap2*Δ clones. Total RNA was extracted from the gametocyte fractions obtained from the wild type and *Pbdpap2*Δ clone A in two independent experiments, while total RNA was prepared from *Pbdpap2*Δ clone B gametocytes once. The relative abundances of the *Pbdpap* transcripts were evaluated using the ΔΔ threshold cycle (C_T) method, with the difference between the *Pbdpap* C_T and that of the constitutive control gene A-type 18S rRNA in the wild-type sample as the reference (29). The signal strength from *Pbdpap2* transcripts in the *Pbdpap2*Δ clones was similar to the level in the no-template control, as expected, while there was no difference in the *Pbdpap3* transcript levels between the wild-type and *Pbdpap2*Δ parasite lines (Fig. 2). In contrast, *Pbdpap1* showed >2-fold-higher RNA levels in both clones than in wild-type parasites. One-way ANOVA indicated that this difference was statistically significant ($P = 0.0087$), and further evaluation using Bonferroni's multiple-comparison test found that there was a statistically significant difference ($P < 0.05$) between the wild type and each of clones A and B but not between clones A and B. The results suggest that *dpap1* was significantly upregulated to similar extents (>2-fold) in both the clones and raise the possibility that this increase in *dpap1* was compensating for the loss of *dpap2*.

DPAP2 is insensitive to DPAP1 and -3 inhibitors. To further evaluate the interrelatedness of the 3 DPAPs, 18 inhibitors that had been tested for activity against PfDPAP1 in asexual parasite extracts (see Table S2 in the supplemental material) (15) were evaluated for efficacy against all 3 PbDPAP forms using schizont and gametocyte extracts from wild-type *P berghei* ANKA in an *in vitro* competitive enzymatic assay (Fig. 3A). PbDPAP1 and PfDPAP1 had similar inhibition profiles (15), suggesting that they are orthologues and likely to have similar functions in the two strains. Conversely, only a general DPAP inhibitor, JCP410, inhibited DPAP2 by more than 50% and 5 compounds exhibited 20% inhibition, suggesting structural or functional differences between DPAP1 and -2. One compound, ML4118S, had >1,000 and >100 times more activity against DPAP1 (19 nM) and DPAP3 (0.1 μM), respectively, than against DPAP2 (38.5 μM).

The structural basis for this differential activity was analyzed by comparing the protein structures of DPAP1 and -2 using *in silico* modeling (see Fig. S2 in the supplemental material). *P. falciparum* sequences were used for the modeling, because annotation of *P.*

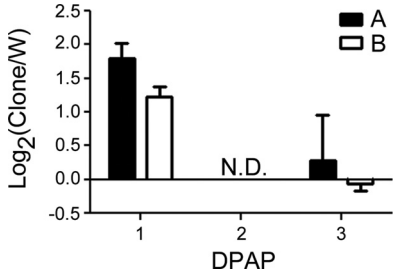

FIG 2 DPAP1, -2, and -3 RT-qPCR. Total RNA was prepared from two independent samples of synchronized, purified gametocytes from wild-type and *Pbdpap2*Δclone A parasites (A; black bars) and one sample from *Pbdpap2*Δ clone B parasites (B; white bars) and the RT-qPCR assay done in triplicate. The $2^{-\Delta\Delta Ct}$ method was used to calculate the relative quantities in relation to the wild-type sample quantity, and the results were plotted as log2 values. The signal from *Pbdpap2* in clones A and B was the same as that from the no-template control and designated not detectable (N.D.).

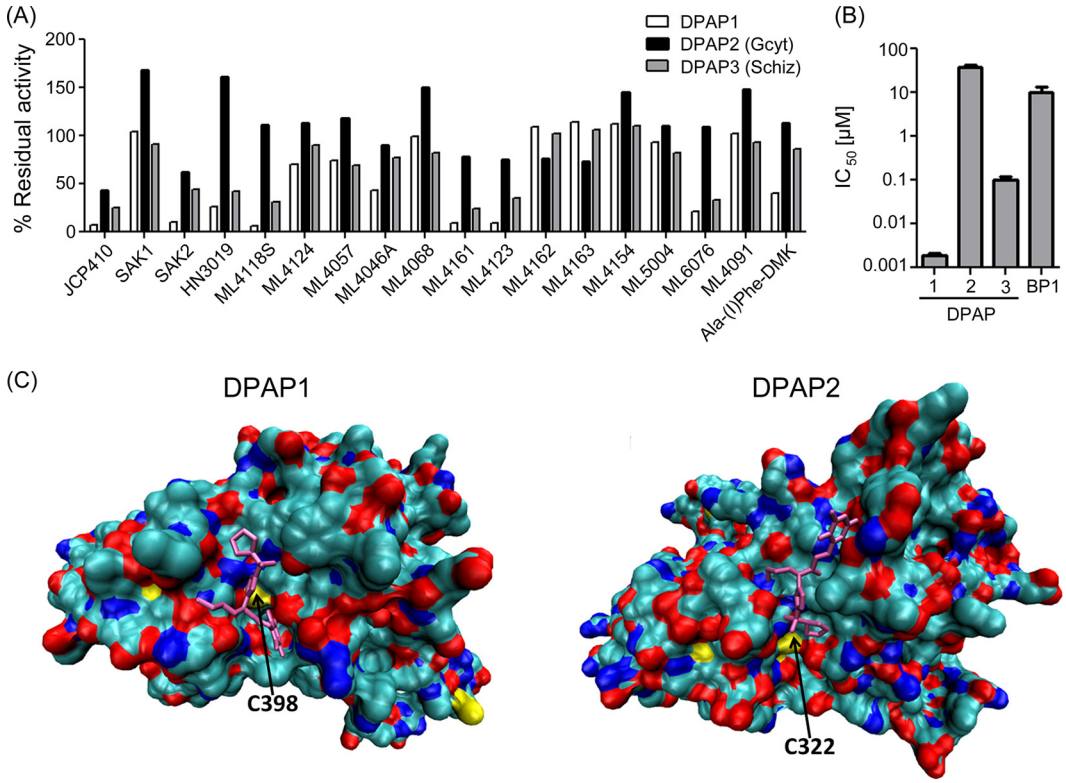

FIG 3 *In vitro* enzymatic assay with DPAP1 inhibitors and *in silico* structure modeling. (A) Inhibition assay with 18 DPAP1 inhibitors. Wild-type schizont and gametocyte lysates were incubated with 1 μM inhibitor or DMSO for 30 min prior to the labeling of residual DPAP activities with the fluorescent activity-based FY01 probe. The signal from the compound-treated sample was normalized to the DMSO control value and plotted on the *y* axis as percent residual activity. (B) Evaluation of the ML4118S IC_{50} for PbDPAP1 to -3 and Berghepain-1 (BP1). (C) ML4118S docked to DPAP1 and DPAP2. The three-dimensional model of DPAP1 and -2 is depicted in a surface representation with colored atom types (carbon = cyan, nitrogen = blue, oxygen = red, and sulfur = yellow). Hydrogen atoms were removed for clarity. The ligand ML4118S is represented in a licorice model and is colored magenta. The positions of the catalytic cysteine residues in DPAP1 and -2 are indicated with black arrows and labeled.

berghei DPAP2 was incomplete. Multiple alignment of protein sequences of *P. falciparum* DPAP1 to -3 suggested significant deviations in the lengths and homologies of DPAP1 and -3 in comparison to those of DPAP2. Three-dimensional structures of DPAP1 and -2 were modeled using the crystal structure of human cathepsin C. Structural superpositioning of DPAP1 and -2 identified regions of large deviations with root mean square deviations of 5.73 Å. DPAP1 has a 55-residue-long insertion region that could not be modeled due to lack of homology to the template. However, molecular refinement of the structure suggests that this loop region probably influences the conformation of the alpha helix that connects the catalytic site to the rest of the structure. This conformational change can be visualized along the length of the helix during the simulations (see Fig. S2 in the supplemental material). These results suggest that the overall structure of DPAP2 is tightly packed and that this has significant influence on the catalytic site, as evidenced by the binding profile of ML4118S. The catalytic site of DPAP1 is well suited to the binding of ML4118S and the formation of a covalent bond with catalytic cysteine—C398 (Fig. 3C)—as well as to favorable interactions with F450, Y399, Q392, V569, and N570. However, in DPAP2 the catalytic site is much more constrained and does not facilitate the binding of ML4118S in a similar mode. Due to this change in binding mode, the ligand would not be predicted to bond to the conserved catalytic cysteine—C322. These results are consistent with ML4118S being more effective against DPAP1 than against DPAP2. In a similar study by Deu et al. (15), the catalytic site of DPAP3 was shown to accommodate large functional groups in comparison to that of DPAP1, suggesting that this region is amenable to the designing of subtype-specific inhibitors of DPAPs.

Effect of DPAP inhibition on oocyst production. The role of PbDPAP1 and -3 during parasite development in the mosquito midgut was assessed using an inhibitor, ML4118S, which has potent activity against both DPAP1 and -3 (Fig. 3A and B) (15). Blood from a mouse infected with *Pbdpap2*Δ clone A parasites was incubated with 10 μM ML4118S or DMSO and then fed to mosquitoes via membrane feeder. A week later, the mosquito midgut was harvested by dissection and the number of *P. berghei* oocysts counted. The median number of oocysts/midgut ($n = 14$) was the same for both treated and nontreated *Pbdpap2*Δ clone A, and there was no significant difference by Mann-Whitney test (Fig. 4). The short 10-min incubation period may not have been sufficient to inactivate the enzyme activity but could not be extended, because the number of oocysts decreases dramatically with longer incubations and the compound cannot be given directly to mice due to toxicity (15).

DPAP1 and -3 inhibitor showed *P. falciparum* gametocytocidal activity. For a more detailed analysis of the role of DPAPs during gametocyte maturation in a parasite that causes malaria in human, the *Pfdpap2*. gene was disrupted in *P. falciparum*.

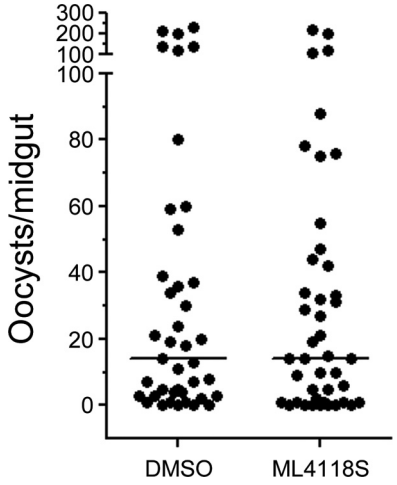

FIG 4 Effect of DPAP inhibitor on oocyst production. Blood was collected from mice infected with *Pbdpap2*Δ clone A and incubated for 10 min at 37°C with DMSO or 10 μM ML4118S, a DPAP1 and -3 inhibitor, before being fed to *A. stephensi* using a membrane feeder. At 11 to 12 days later, the mosquitoes were dissected and the numbers of mercurochrome-stained oocysts counted. The number of oocysts per mosquito midgut is plotted, and the means are indicated by horizontal bars.

After transformation of the wild type (3D7 strain) with pDT.Tg23.*Pfdpap2*1537–2203, a parasite line was isolated with the disruption vector integrated into the *Pfdpap2* locus. The *Pfdpap2*Δ line was viable and produced mature gametocytes, as was seen with the *P. berghei dpap2*Δ clonal lines (Fig. 5A and B), but no transcript for PfDPAP2 was detected in the mutant gametocytes (Fig. 5C). The role of DPAP1 and -3 in gametocyte maturation was then tested by incubation with ML4118S, and the treatment was found to effectively kill 84% of the gametocytes at 10 μM. The effects were similar for the *Pfdpap2*Δ and wild-type lines, suggesting that PfDPAP1 or -3 or both are required for gametocyte maturation (Fig. 5D). However, ML4118S was found to be more effective against asexual stages, blocking *P. falciparum* replication at low nanomolar concentrations (7) and inhibiting PfDPAP1 and -3 activities at submicromolar concentrations (7). It is possible that ML4118S has less access to its targets in gametocytes, since late-stage gametocytes no longer ingest the RBC cytoplasm, and this could result in a lower effective concentration of the compound inside parasites. Also, parasite killing might require longer sustained inhibition of DPAP1 in gametocytes than in the asexual stage (7), thus demanding higher inhibitor concentrations.

To further evaluate whether the gametocytocidal activity of ML4118S was due to DPAP inhibition, we used its diastereomer ML4118R, which has 1,000-fold-lower potency against DPAPs.

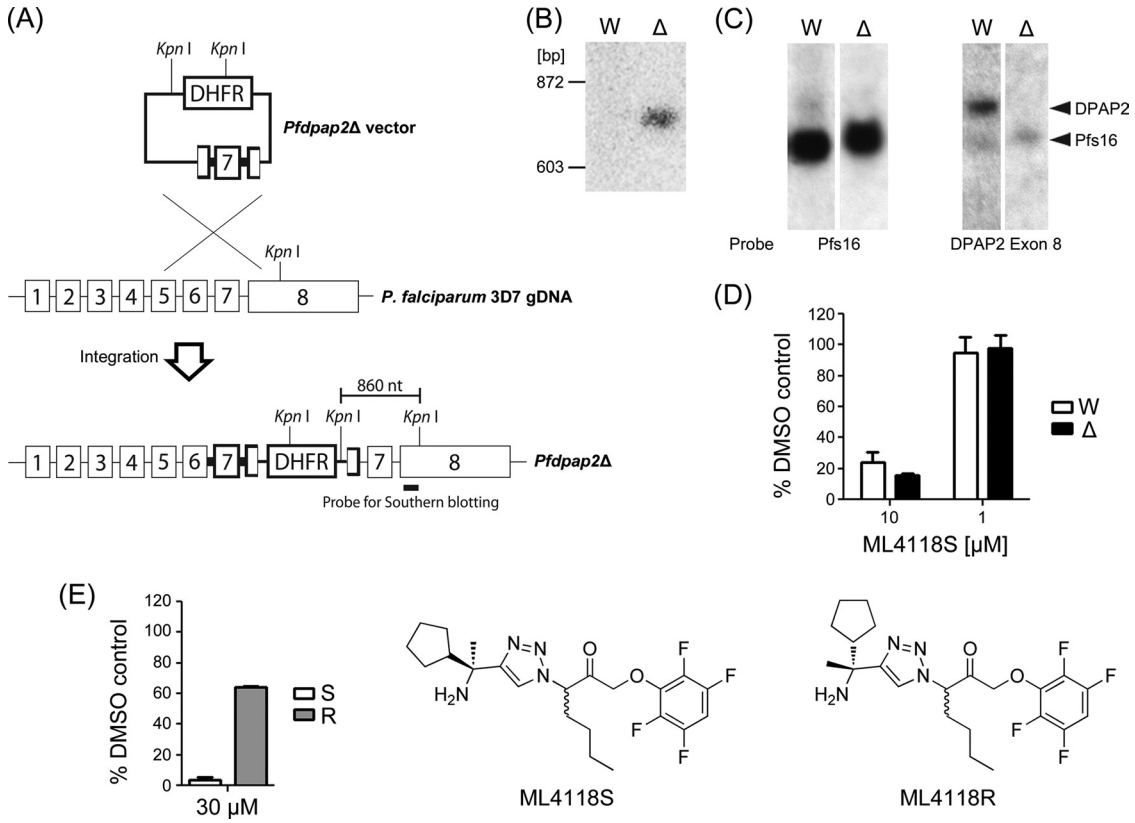

FIG 5 *P. falciparum dpap2* disruption. (A) Schematic of the *Pfdpap2*Δ locus in *P. falciparum*. (B) Southern blotting of KpnI-digested gDNA demonstrating plasmid integration. Wild type, W; *Pfdpap2*Δ clone, Δ. (C) Northern blotting. After probing a Northern blot of RNA isolated from wild-type and *Pfdpap2*Δ parasites with a radiolabeled PCR product corresponding to *Pfs16*, the blot was stripped and probed with a radiolabeled *Pfdpap2* PCR product. The results demonstrate expression of gametocyte-specific transcript *Pfs16* but not *Pfdpap2* in the *Pfdpap2*Δ clone (Δ), while both are expressed in wild-type gametocytes (W). (D) Gametocytocidal *in vitro* drug assay using a DPAP1 and -3 inhibitor, ML4118S, against wild-type gametocytes (W) and *Pfdpap2*Δ gametocytes (Δ). (E) Comparison of the gametocytocidal activities of ML4118S (S) and ML4118R (R), the ML4118S analog which does not inhibit DPAP.

ML4118S reduced gametocyte viability by 97% at 30 μM, in contrast to the reduction by 35% seen for ML4118R at the same concentration (Fig. 5E). Although at these high concentrations these compounds might hit other targets (7), the difference between ML4118R and ML4118S in potency is significant, thus suggesting a possible role for DPAP1 or -3 in gametocyte development.

DISCUSSION

In contrast to the essential functions of DPAP1 and -3 (13, 14), this report shows that deletion of gametocyte-specific DPAP2 in *P. falciparum* and *P. berghei* had no effect on asexual growth, gametocyte production, or *P. berghei* transmission from mouse to mouse via a mosquito. However, ML4118S, which blocks the activity of DPAP1 and -3, did have gametocytocidal activity against *P. falciparum*, suggesting that at least one of these two critical genes could also be required for sexual stage development and thus could be a target for a multistage drug. As additional DPAP1 and -3 inhibitors with a better safety profile in mice become available, it would be interesting to reevaluate their gametocytocidal activity and transmission-blocking potential. The need for micromolar levels of ML4118S to effectively inhibit gametocyte viability, while nanomolar concentrations of ML4118S block DPAP1 and -3 enzymatic activities, warrants further analysis to confirm the target as well as compound accessibility and stability in the gametocytocidal assay. The *dpap2*Δ lines could be used in conjunction with the inhibitors to confirm that DPAP2 does not play a major role and to allow the focus of further drug development on the other DPAPs.

Proteomic data from both *P. berghei* and *P. falciparum* are consistent with the expression of DPAP1 in sexual as well as asexual stages, while DPAP2 expression is limited to the sexual stages and DPAP3 was detected in merozoites (30). Unlike *P. berghei*, to date no *dpap2* homolog has been found in *P. yoelii*, while transcripts for *Pydpap1* (PY05365) and *Pydpap3* (PY01608) have been found in both sexual and mosquito stages (31). It is possible that *dpap2* is not essential but confers a selective advantage for the parasite during the critical transmission stage, which is a major bottleneck in the life cycle (32). In asexual stages, DPAP1 and DPAP3 have been associated with hemoglobin digestion and RBC emergence, respectively, but the work presented here is the first to evaluate their role in other stages of the life cycle.

Unlike the well-defined dependence of intraerythrocytic asexual parasites and early-stage gametocytes on glycolysis and hemoglobin digestion, the major nutritional source used by the parasite during the later stages of gametocyte development and after emergence from the RBC in the mosquito midgut is not known (33–35). Hemoglobin digestion is complete by stage III of gametocytogenesis, as demonstrated by the lack of an effect of cysteine protease inhibitor E64d on food vacuole morphology in stage III to V gametocytes (17, 18), and yet the parasite continues to increase in size, suggesting continued metabolism. Additional support for a metabolic shift during sexual development is provided by a report showing that oocyst production, but not asexual growth, is arrested in type II NADH:ubiquinone dehydrogenase and succinate-ubiquinone oxidoreductase knockout parasites (36, 37). The requirement for these genes indicates the need for the mitochondrial respiratory chain for development in the mosquito, and this could provide an alternative to hemoglobin as an energy source. It is possible that DPAPs also play an important role in peptide degradation in this alternative pathway. This is further supported by the broad substrate specificity of DPAP1 and -3 (13, 14), which indicates a potential to process or degrade different proteins at different points in the parasite life cycle. DPAP1 has activity against a number of peptides with diverse N-terminal amino acids. Peptides starting with proline-arginine are the best substrates, while peptides with basic N-terminal amino acids are not cleaved (13). DPAP3 is also considered a general maturase of secreted proteins, allowing it to potentially play a role in a variety of proteolytic processing events in addition to schizont egress (14).

The distinct inhibitor profiles of the three DPAPs shown in the work presented here demonstrate both similarities and differences in their substrate specificity. All three are labeled with FY01 and inhibited by human cathepsin C inhibitor JCP410, while other compounds such as ML4118S are more effective against DPAP1 and -3 than against DPAP2 in the FY01 competition assay. The lack of efficacy of many of the inhibitors against DPAP2 may be because they were identified by screening against asexual parasites; however, it also suggests that DPAP2 may target a more limited set of substrates than DPAP1 and -3. Direct screening of compound libraries against DPAP2 would be required to determine whether there are DPAP2-specific inhibitors or whether DPAP2 binds only a subset of those that also bind DPAP1 and -3. At the sequence level, DPAP2 is much more closely related to DPAP1 (BLAST analysis; $E < 2e^{-57}$) than to DPAP3 (BLAST analysis; $E < 3e^{-13}$). All three have the conserved cathepsin C active-site residues, QxxxGx CY, GGF, and NH, which is consistent with their ability to complement the activity of DPAP2 in the knockout lines. However, *in silico* structural modeling demonstrated that DPAP1 and -3 have a longer loop region between GGF and NH than either human cathepsin C or DPAP2 (see Fig. S2 in the supplemental material). These additional amino acids could alter the structure of the binding site by shifting the conformation of the alpha helix connecting the catalytic site and the loop region shown (Fig. 3C; see also Fig. S2). This conformational change between DPAP1 and -2 is predicted to alter ML4118S binding so that it could access only the catalytic cysteine residue in DPAP1, not in DPAP2 (Fig. 3C). These preliminary studies provide opportunities to capitalize on the differences between the *P. falciparum* and human enzymes to design parasite-specific compounds.

In summary, we have demonstrated that an inhibitor of DPAP1 and -3, ML4118S, has gametocytocidal activity in wild-type *P. falciparum* parasites as well as in a *Pfdpap2*Δ line. This suggests that DPAP activity could play a role in malaria transmission, in addition to roles in hemoglobin digestion and schizont egress. In contrast, although DPAP2 is specifically upregulated in late-stage gametocytes, it is not essential for gametogenesis or the development of infectious sporozoites. However, DPAP2 could confer a selective advantage under field conditions, which were not replicated in our *in vivo* mouse model. Importantly, the dual effects of ML4118S on asexual and gametocyte viability indicate that analogs with reduced toxicity could have potential as drugs that treat symptoms and block malaria transmission.

ACKNOWLEDGMENTS

This work was supported by the Divisions of Intramural Research at the National Institute of Allergy and Infectious Diseases, National Institutes of Health, and by Public Health Service grants AI40592 and AI48826 from the National Institute of Allergy and Infectious Diseases, National Institutes of Health.

We thank B. Czesny, J. Anigbo, and O. Ayo for technical assistance, M. J. Leyva and J. A. Ellman for providing compounds, S. Kanzok for assistance in setting up the *P. berghei* system, and both S. Kanzok and M. Klemba for helpful discussions.

REFERENCES

1. **malERA Consultative Group on Monitoring, Evaluation, and Surveillance.** 2011. A research agenda for malaria eradication: monitoring, evaluation, and surveillance. PLoS Med. **8:**e1000400. doi:10.1371/journal.pmed.1000400.
2. **Alonso PL, Brown G, Arevalo-Herrera M, Binka F, Chitnis C, Collins F, Doumbo OK, Greenwood B, Hall BF, Levine MM, Mendis K, Newman RD, Plowe CV, Rodriguez MH, Sinden R, Slutsker L, Tanner M.** 2011. A research agenda to underpin malaria eradication. PLoS Med. **8:**e1000406. doi:10.1371/journal.pmed.1000406.
3. **Okell LC, Drakeley CJ, Ghani AC, Bousema T, Sutherland CJ.** 2008. Reduction of transmission from malaria patients by artemisinin combination therapies: a pooled analysis of six randomized trials. Malar. J. **7:**125. doi:10.1186/1475-2875-7-125.
4. **Chen PQ, Li GQ, Guo XB, He KR, Fu YX, Fu LC, Song YZ.** 1994. The infectivity of gametocytes of *Plasmodium falciparum* from patients treated with artemisinin. Chin. Med. J. (Engl) **107:**709–711.
5. **Alano P, Carter R.** 1990. Sexual differentiation in malaria parasites. Annu. Rev. Microbiol. **44:**429–449.
6. **Tanaka TQ, Williamson KC.** 2011. A malaria gametocytocidal assay using oxidoreduction indicator, alamarBlue. Mol. Biochem. Parasitol. **177:**160–163.
7. **Peatey CL, Spicer TP, Hodder PS, Trenholme KR, Gardiner DL.** 2011. A high-throughput assay for the identification of drugs against late-stage *Plasmodium falciparum* gametocytes. Mol. Biochem. Parasitol. **180:**127–131.
8. **Adjalley SH, Johnston GL, Li T, Eastman RT, Ekland EH, Eappen AG, Richman A, Sim BK, Lee MC, Hoffman SL, Fidock DA.** 2011. Quantitative assessment of *Plasmodium falciparum* sexual development reveals potent transmission-blocking activity by methylene blue. Proc. Natl. Acad. Sci. U. S. A. **108:**E1214–E1223.
9. **Roepe PD.** 2009. Molecular and physiologic basis of quinoline drug resistance in *Plasmodium falciparum* malaria. Future Microbiol. **4:**441–455.
10. **Rosenthal PJ.** 2004. Cysteine proteases of malaria parasites. Int. J. Parasitol. **34:**1489–1499.
11. **Goldberg DE.** 2005. Hemoglobin degradation. Curr. Top. Microbiol. Immunol. **295:**275–291.
12. **Dalal S, Klemba M.** 2007. Roles for two aminopeptidases in vacuolar hemoglobin catabolism in *Plasmodium falciparum*. J. Biol. Chem. **282:**35978–35987.
13. **Klemba M, Gluzman I, Goldberg DE.** 2004. A *Plasmodium falciparum* dipeptidyl aminopeptidase I participates in vacuolar hemoglobin degradation. J. Biol. Chem. **279:**43000–43007.
14. **Arastu-Kapur S, Ponder EL, Fonovic UP, Yeoh S, Yuan F, Fonovic M, Grainger M, Phillips CI, Powers JC, Bogyo M.** 2008. Identification of proteases that regulate erythrocyte rupture by the malaria parasite *Plasmodium falciparum*. Nat. Chem. Biol. **4:**203–213.
15. **Deu E, Leyva MJ, Albrow VE, Rice MJ, Ellman JA, Bogyo M.** 2010. Functional studies of *Plasmodium falciparum* dipeptidyl aminopeptidase I using small molecule inhibitors and active site probes. Chem. Biol. **17:**808–819.
16. **Le Roch KG, Zhou Y, Blair PL, Grainger M, Moch JK, Haynes JD, De La Vega P, Holder AA, Batalov S, Carucci DJ, Winzeler EA.** 2003. Discovery of gene function by expression profiling of the malaria parasite life cycle. Science **301:**1503–1508.
17. **Hanssen E, Knoechel C, Dearnley M, Dixon MW, Le Gros M, Larabell C, Tilley L.** 2012. Soft X-ray microscopy analysis of cell volume and hemoglobin content in erythrocytes infected with asexual and sexual stages of *Plasmodium falciparum*. J. Struct. Biol. **177:**224–232.
18. **Czesny B, Goshu S, Cook JL, Williamson KC.** 2009. The proteasome inhibitor epoxomicin has potent *Plasmodium falciparum* gametocytocidal activity. Antimicrob. Agents Chemother. **53:**4080–4085.
19. **Janse CJ, Ramesar J, Waters AP.** 2006. High-efficiency transfection and drug selection of genetically transformed blood stages of the rodent malaria parasite *Plasmodium berghei*. Nat. Protoc. **1:**346–356.
20. **Trager W, Jensen JB.** 1976. Human malaria parasites in continuous culture. Science **193:**673–675.
21. **Ifediba T, Vanderberg JP.** 1981. Complete in vitro maturation of *Plasmodium falciparum* gametocytes. Nature **294:**364–366.
22. **Eksi S, Stump A, Fanning SL, Shenouda MI, Fujioka H, Williamson KC.** 2002. Targeting and sequestration of truncated Pfs230 in an intraerythrocytic compartment during *Plasmodium falciparum* gametocytogenesis. Mol. Microbiol. **44:**1507–1516.
23. **Eksi S, Czesny B, Greenbaum DC, Bogyo M, Williamson KC.** 2004. Targeted disruption of *Plasmodium falciparum* cysteine protease, falcipain 1, reduces oocyst production, not erythrocytic stage growth. Mol. Microbiol. **53:**243–250.
24. **Bell AS, Ranford-Cartwright LC.** 2004. A real-time PCR assay for quantifying *Plasmodium falciparum* infections in the mosquito vector. Int. J. Parasitol. **34:**795–802.
25. **Mølgaard A, Arnau J, Lauritzen C, Larsen S, Petersen G, Pedersen J.** 2007. The crystal structure of human dipeptidyl peptidase I (cathepsin C) in complex with the inhibitor Gly-Phe-CHN2. Biochem. J. **401:**645–650.
26. **Sali A, Blundell TL.** 1993. Comparative protein modelling by satisfaction of spatial restraints. J. Mol. Biol. **234:**779–815.
27. **Phillips JC, Braun R, Wang W, Gumbart J, Tajkhorshid E, Villa E, Chipot C, Skeel RD, Kale L, Schulten K.** 2005. Scalable molecular dynamics with NAMD. J. Comput. Chem. **26:**1781–1802.
28. **Jones G, Willett P, Glen RC, Leach AR, Taylor R.** 1997. Development and validation of a genetic algorithm for flexible docking. J. Mol. Biol. **267:**727–748.
29. **Salanti A, Staalsoe T, Lavstsen T, Jensen AT, Sowa MP, Arnot DE, Hviid L, Theander TG.** 2003. Selective upregulation of a single distinctly structured var gene in chondroitin sulphate A-adhering *Plasmodium falciparum* involved in pregnancy-associated malaria. Mol. Microbiol. **49:**179–191.
30. **Hall N, Karras M, Raine JD, Carlton JM, Kooij TW, Berriman M, Florens L, Janssen CS, Pain A, Christophides GK, James K, Rutherford K, Harris B, Harris D, Churcher C, Quail MA, Ormond D, Doggett J, Trueman HE, Mendoza J, Bidwell SL, Rajandream MA, Carucci DJ, Yates JR, III, Kafatos FC, Janse CJ, Barrell B, Turner CM, Waters AP, Sinden RE.** 2005. A comprehensive survey of the *Plasmodium* life cycle by genomic, transcriptomic, and proteomic analyses. Science **307:**82–86.
31. **Zhou Y, Ramachandran V, Kumar KA, Westenberger S, Refour P, Zhou B, Li F, Young JA, Chen K, Plouffe D, Henson K, Nussenzweig V, Carlton J, Vinetz JM, Duraisingh MT, Winzeler EA.** 2008. Evidence-based annotation of the malaria parasite's genome using comparative expression profiling. PLoS One **3:**e1570. doi:10.1371/journal.pone.0001570.
32. **Alavi Y, Arai M, Mendoza J, Tufet-Bayona M, Sinha R, Fowler K, Billker O, Franke-Fayard B, Janse CJ, Waters A, Sinden RE.** 2003. The dynamics of interactions between *Plasmodium* and the mosquito: a study of the infectivity of *Plasmodium berghei* and *Plasmodium gallinaceum*, and their transmission by *Anopheles stephensi*, *Anopheles gambiae* and *Aedes aegypti*. Int. J. Parasitol. **33:**933–943.
33. **Lang-Unnasch N, Murphy AD.** 1998. Metabolic changes of the malaria parasite during the transition from the human to the mosquito host. Annu. Rev. Microbiol. **52:**561–590.
34. **Francis SE, Sullivan DJ, Jr, Goldberg DE.** 1997. Hemoglobin metabolism in the malaria parasite *Plasmodium falciparum*. Annu. Rev. Microbiol. **51:**97–123.
35. **Lew VL, Tiffert T, Ginsburg H.** 2003. Excess hemoglobin digestion and the osmotic stability of *Plasmodium falciparum*-infected red blood cells. Blood **101:**4189–4194.
36. **Boysen KE, Matuschewski K.** 2011. Arrested oocyst maturation in *Plasmodium* parasites lacking type II NADH:ubiquinone dehydrogenase. J. Biol. Chem. **286:**32661–32671.
37. **Hino A, Hirai M, Tanaka TQ, Watanabe YI, Matsuoka H, Kita K.** 2012. Critical roles of the mitochondrial complex II in oocyst formation of rodent malaria parasite *Plasmodium berghei*. J. Biochem. **152:**259–268.